Scientific Research Publishing

Geomaterials, 2026, 16(3), 127-158
https://www.scirp.org/journal/gm
ISSN Online: 2161-7546
ISSN Print: 2161-7538

Experimental Study of the Diffusion of Nitrate and Sulfate Ions through Concrete in the Case of Underground Water Reservoirs and the Impact on Their Durability

Bienvenu Ebata-Ndion[1,2], Jarlon Brunel Makela[1,2], Stiven Cardelin Marien Mangala[1], Narcisse Malanda[1,2]

[1]Laboratory of Mechanics, Energy and Engineering, Higher National Polytechnic Institute, Marien NGOUABI University, Brazzaville, Republic of the Congo
[2]Higher Institute of Architecture, Building Planning and Public Works, DENIS SASSOU N'GUESSO University, Kintélé, Republic of the Congo
Email: nar6malanda@gmail.com

How to cite this paper: Ebata-Ndion, B., Makela, J.B., Mangala, S.C.M. and Malanda, N. (2026) Experimental Study of the Diffusion of Nitrate and Sulfate Ions through Concrete in the Case of Underground Water Reservoirs and the Impact on Their Durability. *Geomaterials*, **16**, 127-158.
https://doi.org/10.4236/gm.2026.163008

Received: June 2, 2026
Accepted: July 28, 2026
Published: July 31, 2026

Abstract

This study addresses the issue of the efficiency of concrete mix design on the evolution of its microstructure, its physico-mechanical properties, and its behavior with respect to ionic transport under aggressive environmental conditions. Eight concrete formulations (F1 to F8), produced using local aggregates from the cities of Brazzaville (Kombé quarry) and Pointe-Noire (Louvoulou and Mboubissi quarries), were investigated. These formulations differ in the nature of the aggregates (rounded or crushed), the proportion of crushed sand, as well as the water-to-cement and gravel-to-sand ratios. The physico-mechanical properties of the concretes, particularly compressive strength, water-accessible porosity, and bulk density, were characterized at 28 and 90 days and then correlated with the diffusion kinetics of nitrate (NO_3^-) and sulfate (SO_4^{2-}) ions measured over a period of 12 weeks. The results highlight a progressive increase in mechanical strength with curing age, reflecting the continuation of hydration reactions and the gradual densification of the cementitious matrix. This evolution is strongly correlated with the reduction in porosity and the increase in density, thereby confirming that porosity constitutes the essential microstructural parameter controlling the mechanical performance and durability of concrete. Furthermore, the comparative analysis shows that formulations based on crushed aggregates, particularly formulations F1 and F3, develop a more compact microstructure and a denser interfacial transition zone (ITZ) than concretes made with rounded aggregates,

thus limiting preferential diffusion pathways. The diffusion tests also reveal two distinct transport behaviors depending on the nature of the ions studied. Nitrates exhibit a predominantly conservative behavior governed by diffusion, with higher concentrations observed in the most porous concretes. In contrast, sulfates display a non-conservative behavior resulting from a complex coupling between diffusion, chemical reactions, and leaching phenomena. Three transport regimes were therefore identified: a purely diffusive regime, a coupled diffusion-reaction regime, and a regime dominated by the presence of internal ion sources. Finally, the obtained results demonstrate that the durability of concrete cannot be explained solely by conventional mix design parameters, but rather results from complex interactions between microstructure, ionic transport, and chemical reactivity. This study thus highlights the relevance of a performance-based approach founded on physically interpretable parameters for predicting the long-term behavior of concrete intended for underground water reservoirs in humid and polluted environments.

Keywords

Concrete, Durability, Ionic Transport, Diffusion, Microstructure, Porosity, Nitrates, Sulfates

1. Introduction

In the Republic of Congo-Brazzaville, infrastructure development relies heavily on the use of concrete formulated with local aggregates, whose granulometric and morphological characteristics vary significantly depending on the extraction areas. Several previous studies have focused on the mechanical properties and microstructure of these materials [1] [2], notably confirming that formulations based on crushed aggregates exhibit a more compact microstructure and a denser interfacial transition zone (ITZ), as identified by SEM-EDS analyses. However, their behavior with respect to the diffusive transport of aggressive ionic species remains poorly understood or at least insufficiently documented, particularly under conditions representative of humid and polluted environments where these underground structures are installed.

The durability of concrete structures exposed to aggressive environments constitutes a major challenge for the longevity of infrastructures, especially underground hydraulic structures such as water reservoirs [3] [4]. This issue is particularly critical in humid tropical regions, where climatic conditions promote soil saturation, increased interstitial humidity, and intensified migration of pollutants toward buried infrastructures [5]. In such environments, nitrate (NO_3^-) and sulfate (SO_4^{2-}) ions, for example, which are frequently present in contaminated soils, groundwater, or anthropogenic discharges, may progressively penetrate the cementitious matrix by diffusion and interact with the hydrated phases of cement [6]-[8].

These physico-chemical interactions may induce progressive modifications in

the concrete microstructure, notably the dissolution of certain hydrated phases, the precipitation of expansive secondary compounds such as ettringite formed during cement hydration or gypsum, as well as changes in porosity and pore network connectivity [9]-[11]. In the long term, these mechanisms are likely to alter the mechanical properties of the material, accelerate degradation processes, and compromise the durability of these structures [12] [13]. In the specific case of drinking water reservoirs, these phenomena may also affect the quality of the stored water, thereby giving the issue a structural, environmental, and public health dimension [14].

Understanding the mechanisms of ionic transport in cementitious materials, therefore, appears essential for evaluating the long-term behavior of structures exposed to chemically aggressive environments. However, the transfer of ionic species in concrete results from a complex coupling between diffusion, chemical reactions, leaching phenomena, and microstructural evolution [15] [16]. These mechanisms strongly depend on concrete mix design parameters, particularly the water-to-cement ratio, accessible porosity, the nature of the aggregates, and the quality of the interfacial transition zone (ITZ) [17]-[19].

2. Materials and Methods

The approach adopted in this study is based on an experimental methodology aimed at assessing the influence of concrete mix design on durability with regard to nitrate and sulfate ion penetration. Physico-mechanical characterization tests and ionic diffusion experiments were carried out to establish relationships between the microstructural properties of the materials and their transport behavior with respect to aggressive species.

2.1. Physico-Mechanical Characterization

The physico-mechanical properties of the concretes were evaluated at 28 and 90 days in order to analyze the influence of the mix design on the evolution of the microstructure and on ionic transport mechanisms.

The physico-mechanical tests were carried out on cubic specimens measuring $15 \times 15 \times 15$ cm^3, prepared in accordance with NF EN 12390-2 [20]. After demolding at 24 h following storage under moist protection at ambient temperature, the specimens were cured in saturated water until the ages of 28 and 90 days before the characterization tests were performed.

Compressive strength was determined in accordance with NF EN 12390-3 [21] using a hydraulic testing machine applying a continuously increasing monotonic load until specimen failure. This characterization makes it possible to assess the degree of compactness and the quality of the cementitious matrix developed during the hydration process.

Water-accessible porosity, apparent density, and water absorption coefficient were measured using the hydrostatic weighing method in accordance with NF P 18-459 [22]. These parameters constitute essential indicators of the pore structure

of concrete, since porosity and the connectivity of the capillary network play a decisive role in moisture and ionic transport phenomena.

For each mix design, three specimens were tested for each characterization method performed (compressive strength, water-accessible porosity, water absorption, and apparent density) at both 28 and 90 days.

The methodological approach adopted in this study is based on a multi-scale perspective aimed at establishing correlations between the intrinsic properties of concretes, particularly porosity, density, and mechanical performance, and their behavior with respect to the diffusive transport of aggressive species.

2.2. Experimental Diffusion Simulations

2.2.1. Laboratory Experimental Setup

To realistically reproduce the contamination conditions of water stored in underground reservoirs, a specific experimental setup was designed to investigate the diffusive transport of nitrate (NO_3^-) and sulfate (SO_4^{2-}) ions through concrete walls. The experimental system is based on a configuration coupling a contaminated medium with a concrete tank containing drinking water, thereby generating and maintaining a concentration gradient representative of actual service conditions. This arrangement aims to simulate, under controlled conditions, the ionic migration mechanisms that may affect the quality of the stored water.

The diffusion tests were carried out in eight rectangular polymer containers measuring 0.30 m × 0.50 m. Each container housed a concrete tank intended for drinking water storage, with internal dimensions of 0.25 m × 0.35 m and a uniform wall thickness of 0.05 m. The annular space between the concrete tank and the outer container was filled with fine sand saturated with the contaminant solution, with a width of approximately 7.5 cm in the longitudinal direction and 5 cm in the transverse direction. The tanks were manufactured using the different concrete mix designs investigated and were cured under moist conditions for 28 days in accordance with the requirements of NF EN 12390-2 [20].

The external aggressive solution was prepared from stock nitrate and sulfate solutions and subsequently diluted in diffusion tanks with a volume of 25 L. For nitrates, a stock solution with a concentration of 2.5 g/L was used. A volume of 300 mL was then withdrawn and diluted in 25 L of distilled water to obtain an initial concentration of 30 mg/L. Similarly, for sulfates, a stock solution with a concentration of 4.334 g/L was prepared; 300 mL of this solution was diluted in 25 L of distilled water to obtain an initial concentration of 52 mg/L.

The concentrations in the diffusion tanks were maintained constant throughout the test period by renewing the external solution every two weeks during the twelve weeks of exposure. All experiments were conducted in an air-conditioned laboratory at a controlled temperature of 23 ± 2˚C.

2.2.2. Experimental Procedure

Chemical analyses were performed using a DR 7100 UV-Visible spectrophotometer (**Figure 1**), which allows the quantitative determination of dissolved species

through absorbance measurements in accordance with the Beer-Lambert law. The analytical wavelengths were selected according to the characteristic absorption maxima of the species under investigation.

Figure 1. DR 7100 spectrophotometer.

Nitrate Analysis Procedure

Nitrate concentrations were determined using the HACH colorimetric method, based on the principles of ISO 7890, with the NitraVer® 5 reagent (ref. 14034-99), following the manufacturer's recommended procedure (HACH, 2023) [23]. After adding the reagent to 10 mL of the sample, the mixture was shaken for one minute and then allowed to react for five minutes. Absorbance was subsequently measured at a wavelength of 520 nm. The method provides a measurement range from 0.3 to 30 mg/L NO_3^-. The detection limit was not reported by the manufacturer in the available technical documentation.

Sulfate Analysis Procedure

Sulfate concentrations were determined using the HACH turbidimetric method, based on the principles of NF T90-040, with the SulfaVer® 4 reagent (ref. 21067-69), following the manufacturer's recommended procedure (HACH, 2023) [23]. After adding the reagent to 10 mL of the sample, the mixture was shaken for one minute and then allowed to react for five minutes. Absorbance was measured at a wavelength of 650 nm. The method covers an analytical range from 2 to 70 mg/L SO_4^{2-}. The detection limit was not reported by the manufacturer in the available technical documentation. The low sulfate concentrations measured, which were close to the quantification limit of the method, were used primarily to compare the relative diffusion trends among the different concrete formulations rather than for absolute sulfate quantification.

The collected samples were homogenized prior to analysis. When necessary, samples were filtered to remove suspended particles that could interfere with optical measurements.

The calibration curves used were those integrated into the spectrophotometer and validated by the manufacturer for the corresponding analytical methods. Before each series of measurements, the instrument was checked using a blank prepared with distilled water.

Samples with concentrations exceeding the analytical range of the method were diluted with distilled water using a dilution factor of 10. The concentrations obtained after analysis were subsequently multiplied by this factor to determine the actual concentrations in the original samples. For each sampling event, three independent measurements were performed. The reported concentrations correspond to the mean values obtained, while standard deviations and coefficients of variation were calculated to assess experimental variability and measurement reproducibility.

The concentrations presented in this study correspond to those measured in the drinking water stored inside the concrete reservoirs. Nitrate- or sulfate-contaminated solutions were applied exclusively to the exterior side of the reservoir walls through the saturated sand medium. Consequently, the measured concentrations reflect the amount of ions that diffused through the concrete wall under the effect of the concentration gradient.

All these measurements (Figure 2 and Figure 3) made it possible to characterize the diffusion kinetics of the contaminant species and to highlight differences in behavior among the concrete formulations investigated.

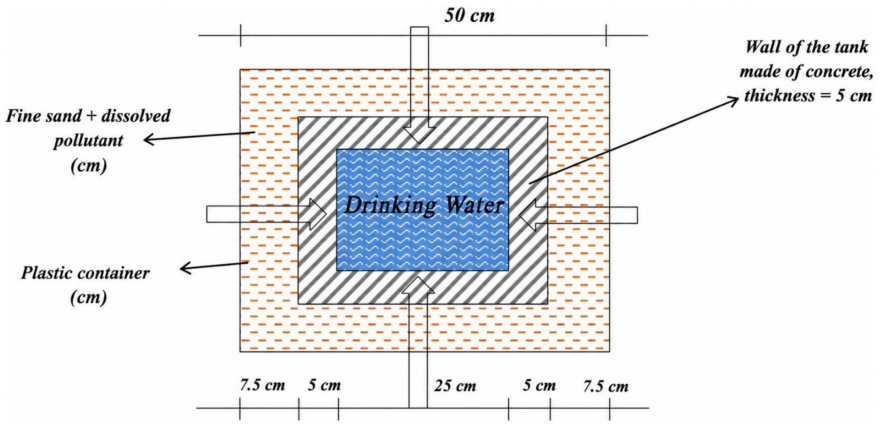

Figure 2. Simplified schematic diagram of the experimental diffusion setup [5].

Figure 3. Overview of the experimental setup and transfer interfaces.

2.3. Presentation of the Data

The studied formulations are primarily distinguished by the nature and size of the aggregates, contrasting rounded aggregates with crushed aggregates, as well as by the geographical origin of the materials, which results in differentiated mineralogical and morphological characteristics. They also vary according to the proportion of crushed sand, ranging from 30% to 50%, introduced in order to optimize grading and improve the compactness of the granular skeleton.

Furthermore, the water-to-cement (W/C) and gravel-to-sand (G/S) ratios were adjusted to ensure comparable workability between the different formulations while inducing controlled variations in the microstructure. These parameters are well known to be decisive in the structuring of the concrete pore network and in the transport mechanisms of aggressive ionic species [3] [4].

In total, eight (8) concrete formulations were studied at 28 days of age using the Dreux-Gorisse mix design method. The different formulations are mainly distinguished by the sources and types of aggregates used [1]:

Formulation 1: composed of a mixture of two classes of crushed aggregates (10/14 and 5/15) sourced from the Kombé quarry in Brazzaville, combined with natural sand from the Congo River.

Formulation 2: identical to Formulation 1, but with sand improved by the addition of 50% crushed sand derived from Inkissi sandstone (Kombé quarry, Brazzaville).

Formulation 3: composed of the same crushed aggregates as the previous formulations, combined with natural sand from the Mfilou River.

Formulation 4: similar to Formulation 3, but with Mfilou River sand enriched with 40% crushed sand.

Formulation 5: produced using a single class of rounded aggregate (3/8) from the Boubissi quarry, along with local natural sand.

Formulation 6: similar to Formulation 5, but using an improved sand composed of 50% crushed sand.

Formulation 7: made with crushed aggregates from the Louvouvou quarry and natural sand from the same region.

Formulation 8: identical to Formulation 7, but with improved sand containing 50% crushed sand.

3. Results and Interpretation

The studies carried out by Makela *et al.* [1] led to compressive strength results measured at 28 days. In the present study, an additional evaluation of compressive strength at 90 days is included, allowing a better understanding of the long-term mechanical behavior of the different concrete formulations investigated. At 90 days, concrete typically reaches about 110% to 120% of its nominal strength, providing increased safety and durability.

The results obtained for the eight formulations are summarized in **Table 1**, which presents the compressive strength values at 90 days of age as well as the

main physico-mechanical properties associated with each formulation.

Table 1. Physico-mechanical characteristics of the concretes studied at 90 days of age.

Formulation	Compressive strength (MPa)	Theoretical density (g/cm³)	Measured density (g/cm³)	Water-to-cement ratio (W/C)	Gravel-to-sand ratio (G/S)	Slump (cm)	Consistency
Formulation 1 (F1)	37.13	2.37	2.43	0.49	2.45	6	Plastic
Formulation 2 (F2)	29.32	2.38	2.38	0.49	1.80	6	Plastic
Formulation 3 (F3)	40.43	2.37	2.45	0.49	2.43	7	Plastic
Formulation 4 (F4)	29.98	2.37	2.41	0.49	1.70	6	Plastic
Formulation 5 (F5)	25.08	2.36	2.30	0.47	3.06	7	Plastic
Formulation 6 (F6)	22.88	2.35	2.28	0.47	1.70	9	Plastic
Formulation 7 (F7)	32.12	2.38	2.38	0.49	2.36	9	Plastic
Formulation 8 (F8)	32.67	2.37	2.37	0.49	1.89	6	Plastic

Figure 4 shows a systematic increase in compressive strength between 28 and 90 days for all formulations, confirming the continuation of hydration reactions and the progressive densification of the cementitious matrix.

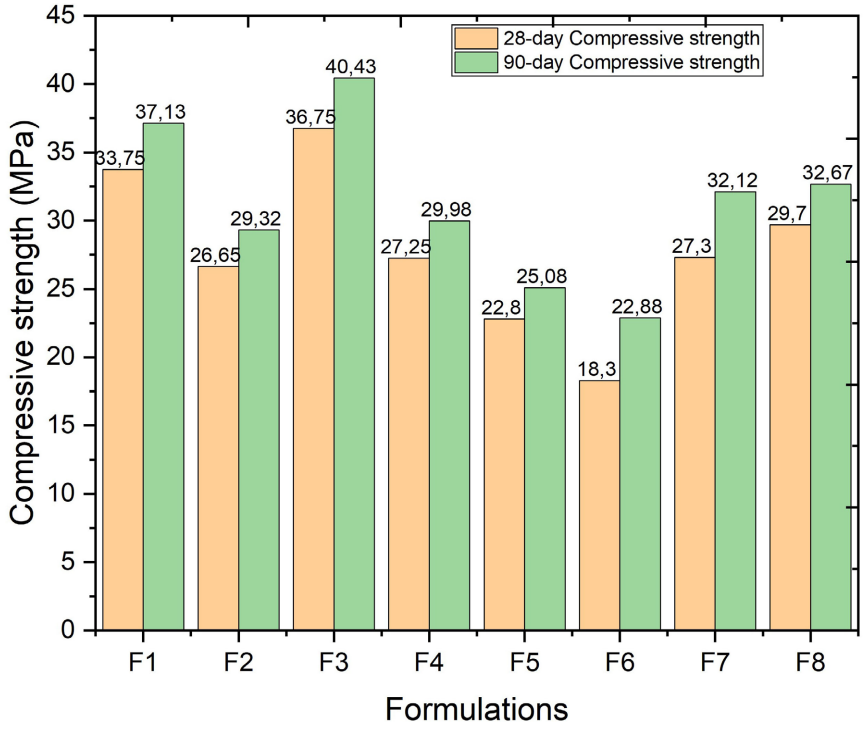

Figure 4. Evolution of compressive strength at 28 and 90 days of concrete.

At 28 days, the compressive strengths range from 18.30 MPa (F6) to 36.75 MPa (F3), whereas at 90 days they vary between 22.88 MPa (F6) and 40.43 MPa (F3). Formulations F3 (36.75 → 40.43 MPa) and F1 (33.75 → 37.13 MPa) exhibit the

highest performance levels, while F5 (22.80 → 25.08 MPa) and F6 (18.30 → 22.88 MPa) show the lowest strengths. The intermediate formulations, such as F8 (29.70 → 32.67 MPa), F7 (27.30 → 32.12 MPa), F4 (27.25 → 29.98 MPa), and F2 (26.65 → 29.32 MPa), reflect moderate levels of compactness.

The strength gains between 28 and 90 days, ranging from +2.28 MPa (F5) to +4.82 MPa (F7), reflect variable hydration kinetics, directly influenced by the nature of the aggregates, the W/C and G/S ratios, as well as the initial density of the material. Figure 4 illustrates this overall evolution and highlights the correlation between microstructural densification, reduction in capillary porosity, and development of mechanical properties. These parameters are not only decisive for long-term performance but also for ionic transport mechanisms and concrete durability. This ranking provides a solid experimental basis for the analysis of ionic diffusion phenomena addressed in the following sections.

3.1. Water-Accessible Porosity and Microstructure

Water-accessible porosity is an essential parameter for assessing concrete durability, as it is directly related to ionic transport mechanisms. It was measured at 28 and 90 days for all formulations.

Figure 5 shows a systematic decrease in porosity between 28 and 90 days, associated with the progressive clogging of capillary pores by hydration products. Concretes F1, F3, and F8 exhibit the lowest porosity values at 90 days (8.2% - 9.0%), indicating a compact microstructure favorable to durability, whereas F5 and F6 show the highest values (10.8% - 14.2%), reflecting a more open structure.

In parallel, the intermediate formulations F2 (10.2%), F4 (9.4%), and F7 (9.2%) exhibit moderate porosity at 90 days, reflecting a balance between granular compactness and capillary network development.

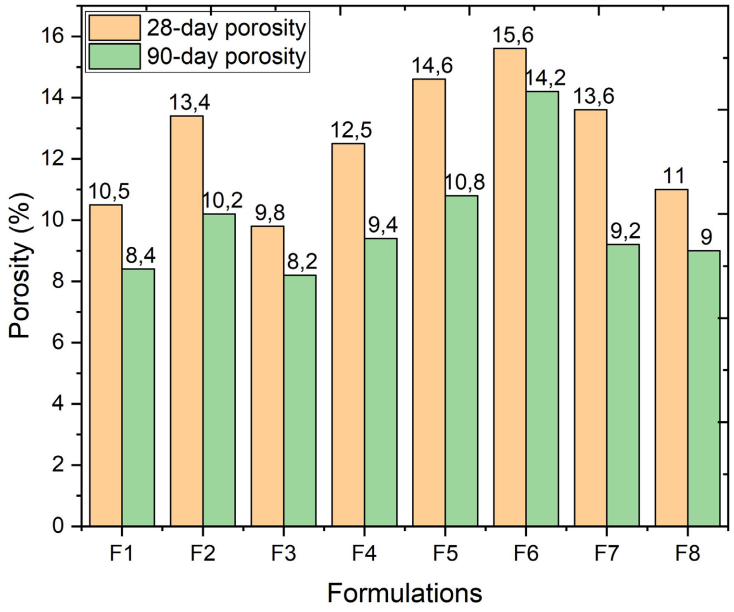

Figure 5. Evolution of porosity of the formulations at 28 and 90 days.

This figure also highlights the ranking of concretes and the correlation between matrix densification and pore network structuring. The most compact formulations (F3, F1, F8) exhibit a limited ionic transport potential, whereas the most porous ones (F5, F6) promote a more open network. The intermediate formulations (F2, F4, F7) reflect a compromise between granular compactness and capillary network development, emphasizing the influence of microstructure on durability. The observed differences in porosity between formulations suggest that concrete microstructure, and more specifically the density of the pore network, is strongly governed by the nature and size of the aggregates, thus justifying a more in-depth analysis of their influence on material structuring and durability.

Relationship between porosity, bulk density, and water absorption.

The combined analysis of water-accessible porosity, bulk density, and water absorption coefficient highlights consistent microstructural relationships that directly reflect the organization of the pore network within the studied materials. These three closely interdependent parameters make it possible to establish an explicit link between compactness, capillary connectivity, and water transport capacity. The corresponding values for the different formulations, determined at 90 days, are summarized in Table 2.

Table 2. Water-accessible porosity, bulk density, and water absorption at 28 and 90 days.

Formulation	Porosity at 28 days (%)	Bulk density at 28 days (g/cm^3)	Water absorption at 28 days (%)	Porosity at 90 days (%)	Bulk density at 90 days (g/cm^3)	Water absorption at 90 days (%)
F3	9.8	2.39	10.86	8.2	2.43	8.93
F1	10.5	2.37	11.73	8.4	2.42	9.17
F8	11.0	2.36	12.36	9.0	2.41	9.89
F7	13.6	2.29	15.74	9.2	2.41	10.13
F4	12.5	2.32	14.29	9.4	2.40	10.37
F2	13.4	2.30	15.47	10.2	2.38	11.36
F5	14.6	2.26	17.10	10.8	2.36	12.11
F6	15.6	2.24	18.48	14.2	2.27	16.55

The examination of these results clearly shows that an increase in porosity, ranging in this study from 8.2% to 14.2%, is systematically accompanied by a decrease in bulk density, which varies from 2.43 g/cm^3 for the most compact formulations to 2.27 g/cm^3 for the most porous ones. This evolution reflects a progressive reduction in material compactness, linked to the increase in void volume within the cementitious matrix.

In parallel, this increase in porosity leads to a significant rise in the water absorption coefficient, ranging from approximately 8.93% to 16.55%. This trend highlights an increase in pore network connectivity, favoring fluid penetration and transport.

Formulations F1, F3, and F8 exhibit the most favorable combinations, combining low porosity (8.2% - 9.0%), high density (≈2.41 - 2.43 g/cm^3), and low absorption (≈9% - 10%), characteristics of a dense and low-permeability microstructure. In contrast, formulations F5 and F6, with higher porosity levels (10.8% - 14.2%), show significantly higher absorption values (>12%), reflecting an open and highly interconnected pore structure.

Figure 6 illustrates these relationships through a cross-representation of the parameters, highlighting the overall trends observed.

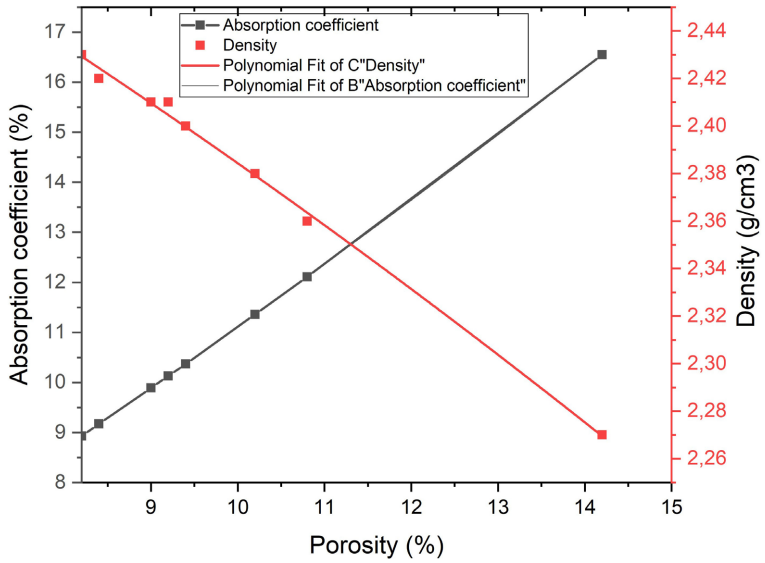

Figure 6. Relationship between porosity, bulk density, and water absorption coefficient.

This graphical representation confirms the existence of an inverse correlation between porosity and bulk density, as well as a positive correlation between porosity and water absorption. It also highlights that bulk density and absorption are complementary manifestations of the same microstructural phenomenon, namely the degree of compactness and the continuity of the pore network.

Thus, porosity appears as the governing parameter of the material's physical behavior, simultaneously controlling macroscopic compactness and water transport capacity. This interdependence gives porosity a central role in interpreting durability performance, particularly with respect to diffusion mechanisms and the penetration of aggressive agents.

These observations highlight the structuring role of the microstructure. It therefore becomes necessary to identify the mix design parameters responsible for these variations, in particular the nature of the aggregates and the granular ratios.

Influence of aggregates on porosity

The nature and size of aggregates are major parameters that govern the microstructure of concrete and, consequently, water-accessible porosity and durability. To highlight their direct impact on porosity and 90-day compressive strength, the key values are summarized in Table 3 below.

Table 3. Porosity and strength of the formulations according to aggregate type.

Formulation	Type of gravel	Porosity at 90 days (%)	Compressive strength at 90 days (MPa)
F1	Crushed aggregate	8.4	37.13
F2	Crushed aggregate	10.2	29.32
F3	Crushed aggregate	8.2	40.43
F4	Crushed aggregate	9.4	29.98
F5	Rounded aggregate	10.8	25.08
F6	Rounded aggregate	14.2	22.88
F7	Crushed aggregate	9.2	32.12
F8	Crushed aggregate	9.0	32.67

At 90 days, mixtures F1 - F4 and F7 - F8, using crushed aggregates from the Kombé and Louvoulou quarries, exhibit low to moderate porosity (8.2% - 9.4%) associated with high compressive strengths (32.12 - 40.43 MPa), whereas mixtures F5 and F6, incorporating 3/8 rounded gravel from the Boubissi quarry in Pointe-Noire, show higher porosity values (10.8% - 14.2%) and lower strengths (22.88 - 25.08 MPa), highlighting the decisive influence of aggregate type and size on the densification of the cement matrix and the potential for ionic transport.

These results confirm that aggregates are key parameters in microstructural control, particularly at the level of the Interfacial Transition Zone (ITZ) [17], recognized as a major factor in concrete durability

Influence of the Gravel-to-Sand ratio (G/S) and Water-to-Cement ratio (W/C) on porosity

Beyond the nature of aggregates, mix design parameters, particularly the gravel-to-sand (G/S) and water-to cement (W/C) ratios, strongly influence the compactness and pore structure of concrete.

To analyze the influence of these parameters on the porosity of the studied concretes, the values of the G/S ratio, W/C ratio, and measured porosity at 90 days are summarized in **Table 4**.

Table 4. Mix design parameters and 90-day porosity of the studied concretes.

Formulations	G/S	W/C	Porosity at 90 days (%)
F1	2.45	0.49	8.4
F2	1.80	0.49	10.2
F3	2.43	0.49	8.2
F4	1.70	0.49	9.4
F5	3.06	0.47	10.8
F6	1.70	0.47	14.2
F7	2.36	0.49	9.2
F8	1.89	0.49	9.0

The analysis of these results shows that mixtures characterized by a relatively balanced G/S ratio, ranging between 1.89 and 2.45, combined with a W/C ratio close to 0.49, develop a more compact microstructure and exhibit lower long-term porosity levels.

Indeed, mixtures F1 (G/S = 2.45), F3 (G/S = 2.43), and F8 (G/S = 1.89) present the lowest porosities at 90 days, namely 8.4%, 8.2%, and 9.0%, respectively, reflecting better granular packing and a bulk density closer to the theoretical density. This configuration promotes a denser arrangement of the cementitious matrix and a reduction of the capillary pore network.

In contrast, mixtures with a more unbalanced G/S ratio develop higher porosity levels. This is particularly the case for concretes F5 (G/S = 3.06) and F6 (G/S = 1.70), which exhibit the highest porosities at 90 days, reaching 10.8% and 14.2%, respectively, despite a slightly lower W/C ratio (0.47). This observation highlights that optimizing the aggregate skeleton can be as decisive as the water-to-cement ratio in structuring the pore network.

However, it should be noted that F4 and F6 share the same G/S ratio (1.70) but show very different porosity values (9.4% vs 14.2%), illustrating that G/S alone is not sufficient to predict compactness: the nature and morphology of aggregates (crushed aggregate for F4 vs rounded gravel for F6) also play a key role, by locally influencing the density of the paste-aggregate interfacial transition zone (ITZ).

These results confirm that an increase in initial water content or an imbalance in the G/S ratio promotes the formation of a more connected capillary network, leading to increased porosity and enhanced diffusive transport mechanisms in concrete.

3.2. Nitrate Diffusion

The analysis of the experimental data (Table 5) shows a progressive and nearly monotonic increase in nitrate concentrations for all mixtures over time. This evolution reflects the continuous penetration of nitrate ions into the cementitious matrix, characteristic of transport dominated by diffusion.

Table 5. Experimental concentrations of nitrate ions (mg/L) in the different concrete mixtures over 12 weeks.

Week	F1	F2	F3	F4	F5	F6	F7	F8
1st week	0.32	0.68	0.28	0.56	0.82	0.98	0.46	0.38
2nd week	0.36	0.72	0.32	0.60	0.86	1.02	0.50	0.42
3rd week	0.41	0.77	0.37	0.70	0.91	1.07	0.55	0.47
4th week	0.46	0.82	0.42	0.76	0.96	1.12	0.60	0.52
5th week	0.52	0.88	0.48	0.82	1.02	1.18	0.66	0.58
6th week	0.58	0.94	0.54	0.89	1.08	1.24	0.72	0.64
7th week	0.64	1.01	0.61	0.96	1.15	1.31	0.79	0.71
8th week	0.71	1.08	0.68	1.03	1.22	1.38	0.86	0.78

Continued

9th week	0.78	1.15	0.75	1.10	1.29	1.45	0.93	0.85
10th week	0.83	1.22	0.80	1.17	1.36	1.56	1.00	0.92
11th week	0.90	1.32	0.85	1.17	1.49	1.72	1.07	0.99
12th week	1.01	1.44	0.97	1.25	1.63	1.88	1.15	1.07

These results clearly show that mixtures F6, F5, and F2 present the highest concentrations, indicating greater permeability of the cementitious matrix and therefore a higher ease of nitrate ion migration. Conversely, F3, followed by F1 and F8, exhibits the lowest concentrations, reflecting better resistance to diffusion. This analysis of concentration variations (Figure 7) highlights the time-dependent effect on nitrate retention in concrete. The interpretation of these results may provide valuable insights into the performance of each mixture in terms of pollutant diffusion and durability.

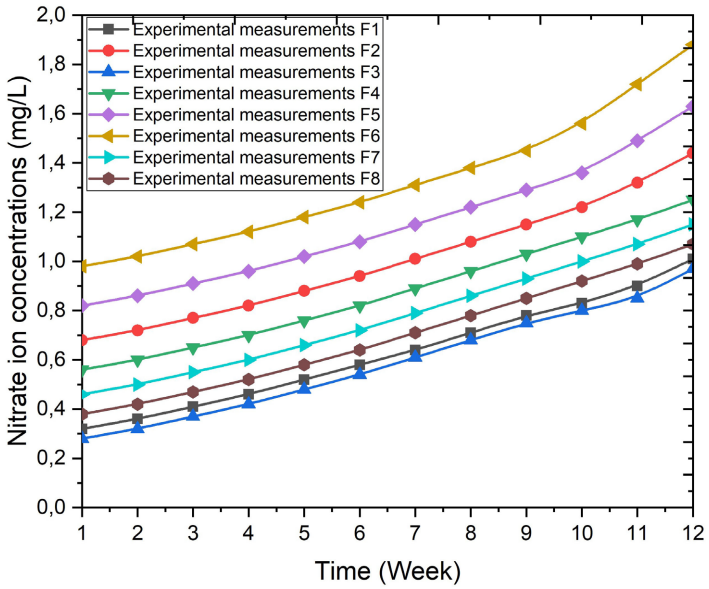

Figure 7. Time evolution of nitrate ion concentrations in the concrete mixtures.

The analysis of the mixtures (Figure 7) shows that concrete composition strongly influences nitrate ion diffusion. The nature of the sand is the most dominant factor, followed by the particle size distribution and the type of coarse aggregates.

A compact granular skeleton, associated with the use of natural sands, helps reduce porosity and pore connectivity, thereby limiting nitrate migration, whereas the use of crushed sands tends to enhance ionic transport. Overall, the mixture composition strongly governs nitrate diffusion. The nature of the sand is the primary influencing factor, followed by grading proportions and coarse aggregate type. A dense granular skeleton combined with natural sands reduces porosity and pore connectivity, limiting nitrate migration, while crushed sands promote ion transport.

3.3. Transport of Sulfate Ions (SO_4^{2-})

Unlike nitrate ions, whose behavior is essentially conservative, sulfate ions exhibit intrinsically reactive transport resulting from a coupling between diffusion and chemical interactions within the cementitious matrix. In cementitious environments, these ions interact with cement hydrates (C-S-H, portlandite) [6], leading to the formation of secondary phases such as gypsum and ettringite. These interactions result in a partial consumption of dissolved ions and modify their effective mobility. Thus, the measured concentrations (**Figure 8**) do not reflect purely diffusive transport but rather an equilibrium between transport, chemical reactions, and, in some cases, internal leaching processes.

It should be noted that when the measured concentration exceeds the initial value C_0 = 52 mg/L, this cannot be explained by external diffusion alone: under steady-state conditions, a purely diffusive incoming flux from a reservoir at concentration C_0 can only lead to concentrations lower than or equal to C_0 in the solution. Any exceedance therefore necessarily implies the existence of an internal source of sulfate ions, independent of the external diffusive flux.

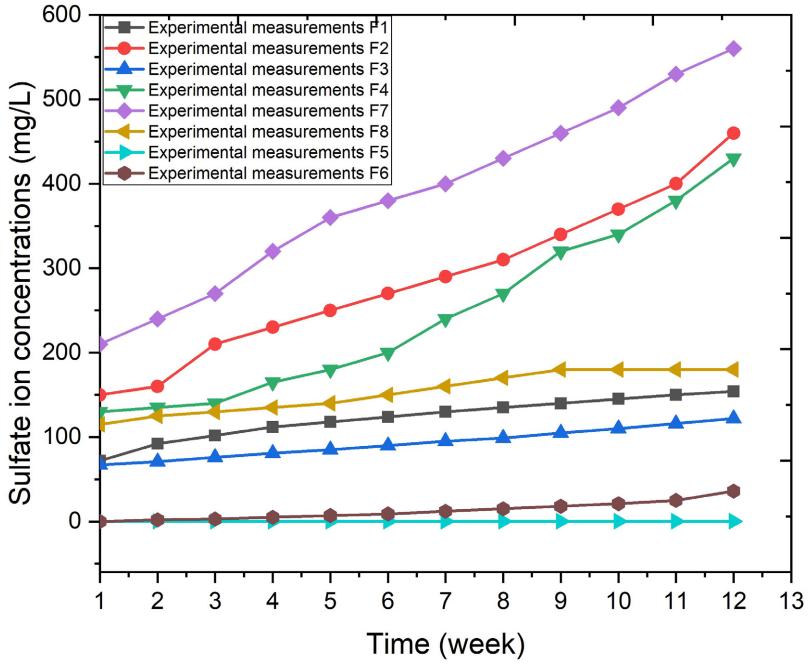

Figure 8. Evolution of sulfate ion (SO_4^{2-}) concentrations in the diffusion tank for mixtures F1 to F8.

The results highlight a structured transition between three transport regimes, directly governed by the microstructural properties of the cementitious materials. The diffusive regime, observed for mixture F6 (**Figure 9**), corresponds to materials characterized by high porosity (ϕ > 13%) and low mechanical strength (Rc < 25 MPa). In this case, the high connectivity of the pore network enhances ionic mobility, and transport is essentially controlled by the concentration gradient.

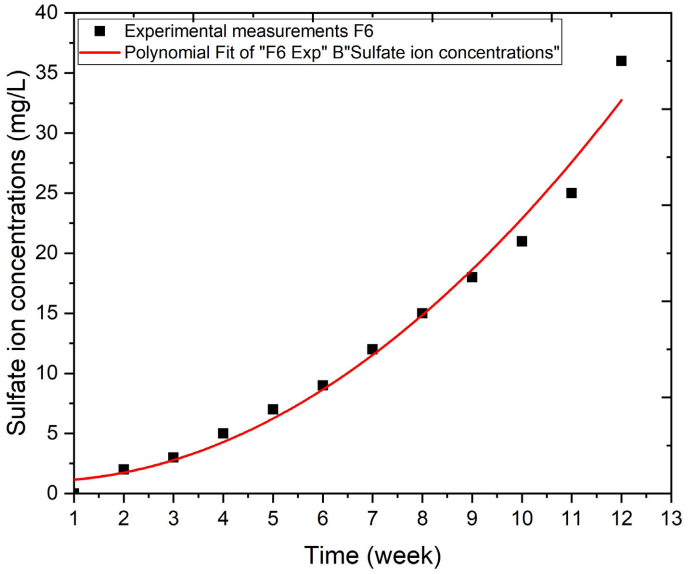

Figure 9. Sulfate ion diffusion kinetics (F6).

The diffusion-reaction coupled regime, illustrated by mixture F5 (**Figure 10**), occurs in materials undergoing densification, with intermediate porosity (≈11% - 13%) and moderate mechanical strength (≈ 25 - 35 MPa). The progressive reduction in pore connectivity limits diffusion, while chemical interactions with hydration products become significant, leading to a partial consumption of sulfate ions.

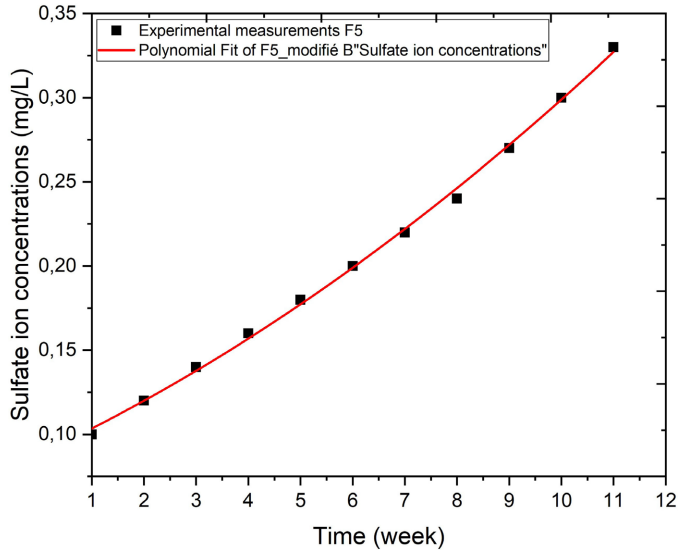

Figure 10. Coupled diffusion-reaction kinetics (mixture F5).

Finally, the regime dominated by internal leaching, characteristic of mixtures F1 - F4, F7, and F8 (**Figure 11**), is observed in denser materials ($\phi \approx 8\%$ - 11%) with higher mechanical strength (Rc ≈ 35 - 40 MPa). In these systems, the limitation of diffusive transport is compensated by the presence of internal ion sources resulting from the destabilization of hydration phases, leading to elevated concen-

trations and non-conservative behavior.

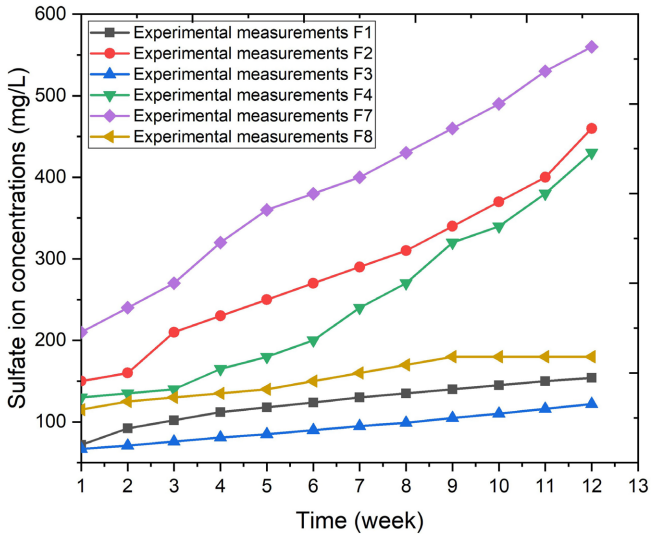

Figure 11. Sulfate ion leaching kinetics for F1 - F4, F7, and F8.

Thus, porosity alone is not a sufficient discriminating criterion. It is the combination of porosity level, pore network connectivity, and compactness state, reflected by mechanical strength, that governs the nature of transport mechanisms.

From this perspective, the transition from a diffusive regime to a coupled regime, and then to a leaching-dominated regime reflects a progressive evolution in transport control. This shifts from a mechanism governed by ionic mobility to a regime where chemical reactivity becomes predominant, and finally to a situation dominated by internal material sources. This transition highlights the intrinsically non-conservative nature of sulfate ion transport, which is strongly dependent on both the microstructure and the chemical stability of the material.

Microstructural correlations and implications for transport

The combined analysis of bulk density, accessible porosity, and compressive strength highlights key structural relationships governing the diffusive behavior of the studied concretes. Measured densities range from 2.25 to 2.45 g/cm^3, accessible porosities from 8.2% to 14.2%, and 90-day compressive strengths from 22.88 to 40.43 MPa. These three parameters, directly linked to material compactness, control both mechanical performance and transport properties. To rigorously interpret these interactions, correlations are examined pairwise.

The relationship between accessible porosity and 90-day compressive strength reveals a clear inverse trend. The most compact mixtures, characterized by low porosity values between 8.2% (F3) and 9.0% (F8), develop the highest mechanical strengths, reaching 40.43 MPa (F3), 37.13 MPa (F1), and 32.67 MPa (F8). Conversely, the most porous concretes, such as F6 (14.2%) and F5 (10.8%), exhibit significantly lower strengths, namely 22.88 MPa and 25.08 MPa, respectively. Intermediate mixtures, including F2 (10.2%; 29.32 MPa) and F4 (9.4%; 29.98 MPa), confirm the continuity of this trend.

Figure 12 highlights a strong negative correlation, confirming that porosity is the governing parameter for mechanical strength. A reduction in porosity from approximately 14% to 8% is associated with an increase in strength of nearly +75%, reflecting densification of the cement matrix and a reduction in capillary connectivity.

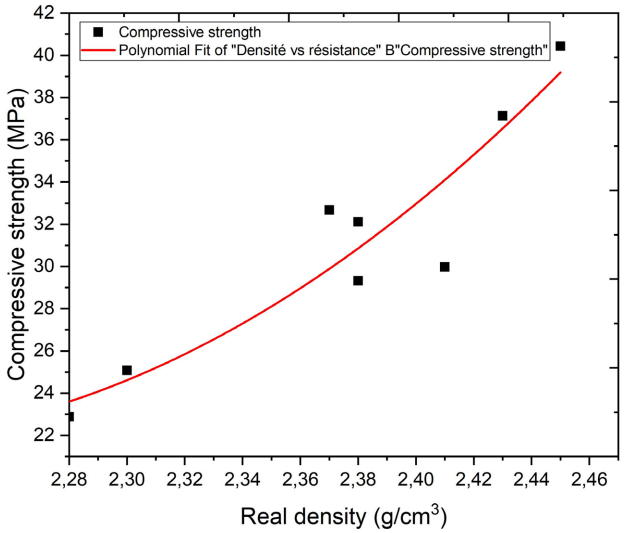

Figure 12. Relationship between accessible porosity (%) and 90-day compressive strength (MPa).

The analysis of the relationship between bulk density and accessible porosity reveals a clear inverse correlation. The densest mixtures, particularly F3 (2.45 g/cm^3) and F1 (2.43 g/cm^3), correspond to the lowest porosity values (8.2% and 8.4%). In contrast, mixtures F6 (2.28 g/cm^3) and F5 (2.30 g/cm^3) exhibit the highest porosities (14.2% and 10.8%). Intermediate mixtures (F2, F4, F7, F8) fall within a density range of 2.37 to 2.41 g/cm^3, associated with porosities between 9.0% and 10.2%.

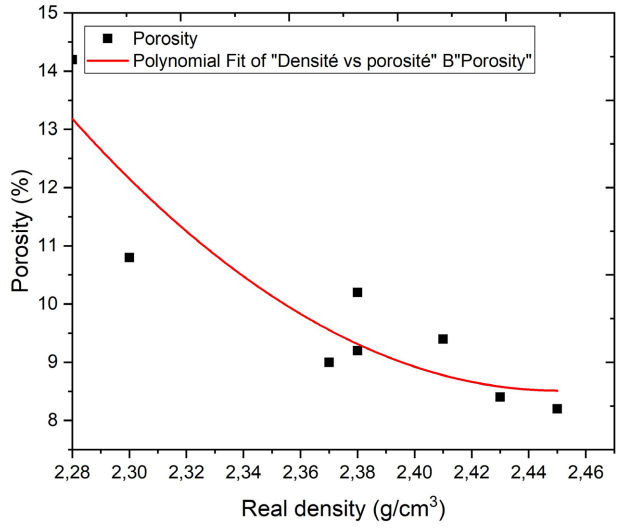

Figure 13. Relationship between bulk density (g/cm^3) and accessible porosity (%).

Figure 13 highlights a significant negative correlation: an increase in density from approximately 2.28 to 2.45 g/cm³ is accompanied by a reduction in porosity from about 14.2% to 8.2%. This relationship confirms that density is a robust indicator of material compactness and underscores the role of aggregate optimization in structuring the pore network.

The relationship between bulk density and compressive strength shows a positive correlation, although less direct than that observed with porosity. The densest concretes, particularly F3 (2.45 g/cm³) and F1 (2.43 g/cm³), develop the highest strengths (40.43 MPa and 37.13 MPa). Conversely, the least dense mixtures, F6 (2.28 g/cm³) and F5 (2.30 g/cm³), exhibit lower strengths (22.88 MPa and 25.08 MPa). The trend observed (Figure 14) shows that an increase in density of approximately +7% (from 2.28 to 2.45 g/cm³) leads to an increase in strength of up to +75%. However, this relationship remains indirect, as porosity acts as the dominant intermediate parameter linking density and strength.

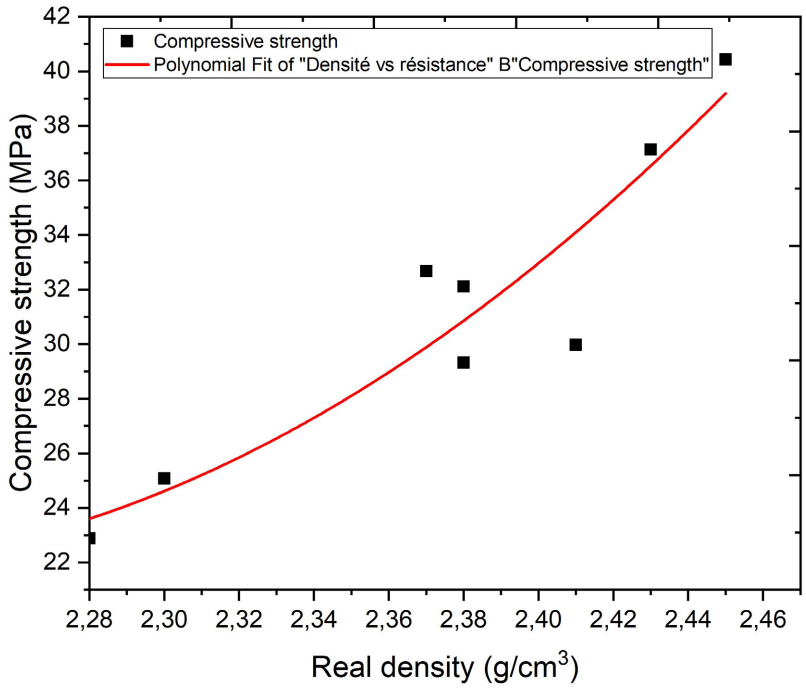

Figure 14. Relationship between bulk density (g/cm³) and 90-day compressive strength (MPa).

Correlation between bulk density, accessible porosity, mechanical strength, and diffusive impact

Table 6 shows that the accessible porosity at 90 days (8.2% - 14.2%) is the key microstructural parameter governing the ranking of ionic transport potential. The most porous mixtures, such as F2 and F6, develop a more connected capillary network, which is favorable to rapid diffusion of ionic species. In contrast, denser concretes, such as F1, F3, and F8, significantly limit diffusive fluxes due to a more compact microstructure.

Table 6. Correlation between bulk density, accessible porosity, mechanical strength, and diffusive impact.

Formulation	W/C	Bulk density (t/m³)	Accessible porosity (%)	Compressive strength at 28 days (MPa)	Compressive strength at 90 days (MPa)	Microstructural analysis	Impact on diffusion
F1	0.49	2.41 → 2.43	10.5 → 8.4	33.75	37.13	Relatively compact microstructure with still-connected capillary network	Slowed diffusion
F2	0.49	2.37 → 2.38	13.4 → 10.2	26.65	29.32	High porosity and significant capillary connectivity	Fast diffusion
F3	0.49	2.44 → 2.45	9.8 → 8.2	36.75	40.43	Dense and poorly connected pore network	Slowed diffusion
F4	0.49	2.39 → 2.41	12.5 → 9.4	27.25	29.98	Relatively continuous capillary network	Moderate to rapid diffusion
F5	0.47	2.26 → 2.30	14.6 → 10.8	22.80	25.08	Porous microstructure with high capillary connectivity	High diffusion
F6	0.47	2.25 → 2.28	15.6 → 14.2	18.30	22.88	Highly open pore network	Very rapid diffusion
F7	0.49	2.37 → 2.38	13.6 → 9.2	27.30	32.12	Relatively dense microstructure with moderate capillary tortuosity	Moderate diffusion
F8	0.49	2.35 → 2.37	11.0 → 9.0	29.70	32.67	Controlled porosity and relatively compact pore network	Moderate diffusion

Figure 15 highlights that the granular skeleton structure and the W/C ratio simultaneously control compactness, porosity, and strength, establishing a direct link with the diffusive transport potential. The intermediate formulations (F2, F4, and F7) lie between these two extremes, illustrating a continuous relationship between microstructure and performance.

Furthermore, formulations F5 and F6 exhibit an open capillary network, characterized by high porosity values (10.8% - 14.2%) and lower densities (2.28 - 2.30 g/cm³), which promote rapid ion diffusion.

The intermediate formulations (F2, F4, and F7) occupy an intermediate position. This visual representation makes it possible to rank the formulations according to their compactness and to anticipate the diffusive behavior of ions.

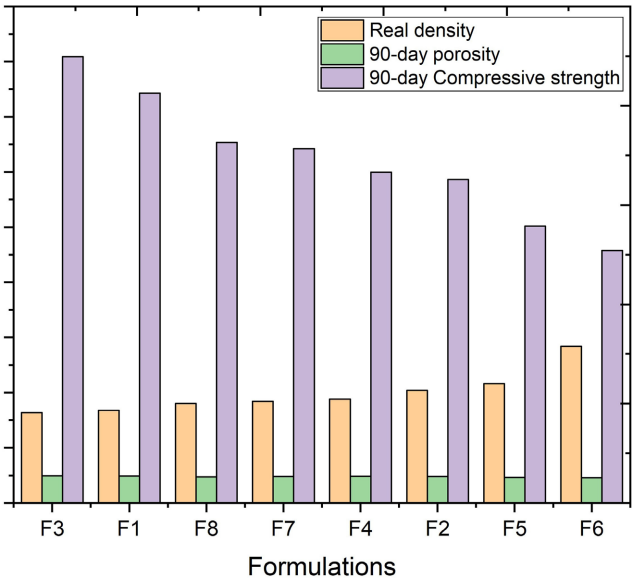

Figure 15. Relationship between porosity, true density, and compressive strength of the formulations.

The observed trends are consistent with the recommendations of EN 206, which specifies maximum water-to-cement (W/C) ratios ranging from 0.45 to 0.55 depending on the exposure class, in order to limit concrete porosity and permeability.

Similarly, ACI 201 [20] emphasizes that the durability of structures exposed to aggressive environments primarily depends on the connectivity of the pore network rather than on mechanical strength alone.

In this context, the measured physico-mechanical properties constitute essential indicators for interpreting ionic transport mechanisms in concrete. In particular, they make it possible to identify formulations that promote rapid diffusion, associated with high porosity and a connected capillary network, as well as those characterized by more limited diffusion due to a dense microstructure.

Formulations F1, F3, and F8, characterized by high densities (2.43 - 2.45 g/cm^3) and low porosities (8.2% - 9.0%), thus develop a compact microstructure favorable to slowed diffusion. In contrast, concretes F5 and F6, which exhibit the lowest densities and the highest porosities (10.8% - 14.2%), possess a more open capillary network that facilitates rapid diffusion of ionic species.

Therefore, the physico-mechanical properties measured in this study should not be regarded solely as indicators of mechanical performance, but also as indirect descriptors of the ionic diffusion potential of concrete. They provide an essential basis for interpreting the transport results presented in the following sections, particularly for distinguishing between behaviors governed by pure diffusion and those involving coupled diffusion-reaction mechanisms.

Microstructure and implications for ionic transport

The correlations highlighted in the previous section reflect fundamental microstructural mechanisms governing the transport behavior of cementitious materi-

als. The combined influence of density, porosity, and mechanical strength can be interpreted at the scale of the pore network, whose geometry, connectivity, and tortuosity directly control diffusive fluxes.

The observed trends are consistent with both normative and theoretical frameworks. EN 206 recommends water-to-cement (W/C) ratios between 0.45 and 0.55 in order to limit capillary porosity and permeability, while ACI 201 [24] emphasizes that the durability of concrete exposed to aggressive environments primarily depends on pore network connectivity rather than on mechanical strength alone.

In this context, accessible porosity appears as the key governing parameter of ionic transport. A decrease in porosity from 14.2% to 8.2% is associated with a significant reduction in capillary connectivity and an increase in pore network tortuosity, resulting in a lower effective diffusion coefficient. True density acts indirectly, reflecting the degree of compaction of the granular skeleton and cement paste, whereas mechanical strength is a macroscopic consequence of this microstructural organization.

The analysis of the formulations confirms this interpretation. Concretes F3, F1, and F8, characterized by high densities (2.43 - 2.45 g/cm^3) and low porosities (8.2% - 9.0%), exhibit a dense microstructure associated with a poorly connected and highly tortuous capillary network. This configuration limits ion penetration and leads to a transport regime governed by slowed diffusion. In contrast, formulations F5 and F6, with lower densities (2.28 - 2.30 g/cm^3) and higher porosities (10.8% - 14.2%), develop a more open and better-connected pore network, favoring rapid ion diffusion.

The intermediate formulations (F2, F4, F7) illustrate transitional microstructural states, in which diffusion is governed by a balance between compactness and capillary connectivity. These intermediate behaviors confirm that ionic transport does not depend on a single parameter, but rather on a multiscale organization of the material. Thus, the measured physico-mechanical properties should not be regarded solely as indicators of mechanical performance, but as indirect descriptors of diffusive transport potential. This interpretation provides a coherent physical framework for analyzing the modeling results presented in the following sections, particularly for distinguishing regimes governed by pure diffusion from those involving coupled diffusion-reaction-leaching mechanisms.

Analysis of Experimental Variability and Robustness of Results

To assess the statistical robustness of the obtained results, each physical, mechanical, and transport property was determined from three independent replicates (n = 3). Standard deviations and coefficients of variation (CV) were calculated for each formulation to quantify measurement dispersion. The summarized results are presented in **Table 7** and **Table 8**, while an overall view of the experimental variability is provided in **Table 9**.

The results presented in **Table 7** highlight a low dispersion of measurements for all the physical and mechanical properties investigated. The coefficients of variation remain below 2% for compressive strength, water-accessible porosity, and water absorption, and below 1% for bulk density. These low levels of dispersion

indicate good repeatability of the tests and confirm the reliability of the mean values obtained.

Table 7. Statistical summary of physical and mechanical properties at 90 days (n = 3).

Formulation	Compressive Strength			Porosity			Water Absorption			Bulk Density		
	Mean (MPa)	Standard Deviation	CV (%)	Mean (%)	Standard Deviation	CV (%)	Mean (%)	Standard Deviation	CV (%)	Mean (g/cm^3)	Standard Deviation	CV (%)
F1	37.13	0.56	1.51	8.40	0.11	1.31	9.12	0.15	1.64	2.43	0.010	0.41
F2	29.32	0.44	1.50	10.20	0.14	1.37	11.20	0.17	1.52	2.37	0.020	0.84
F3	40.43	0.59	1.46	8.20	0.12	1.46	9.05	0.17	1.88	2.42	0.020	0.83
F4	29.98	0.55	1.83	9.40	0.15	1.60	10.52	0.19	1.81	2.39	0.010	0.42
F5	25.08	0.41	1.63	10.80	0.20	1.85	12.25	0.21	1.71	2.35	0.010	0.43
F6	22.88	0.37	1.62	14.20	0.20	1.41	16.20	0.28	1.73	2.28	0.017	0.75
F7	32.12	0.46	1.43	9.20	0.14	1.52	10.25	0.19	1.85	2.41	0.010	0.41
F8	32.67	0.51	1.56	9.00	0.10	1.11	9.95	0.17	1.71	2.40	0.010	0.4

A similar analysis was performed for the ionic concentration measurements obtained at the twelfth week of diffusion.

Table 8. Statistical summary of ionic concentrations at week 12 (n = 3).

Formulation	Nitrates			Sulfates		
	Mean (mg/L)	Standard Deviation	CV (%)	Mean (mg/L)	Standard Deviation	CV (%)
F1	1.01	0.02	1.98	154	3	1.95
F2	1.44	0.03	2.08	460	9	1.96
F3	0.97	0.02	2.06	122	3	2.46
F4	1.25	0.03	2.40	430	8	1.86
F5	1.63	0.03	1.84	0.36	0.01	2.78
F6	1.88	0.04	2.13	36	1	2.78
F7	1.15	0.02	1.74	560	11	1.96
F8	1.07	0.02	1.87	180	4	2.22

The ionic concentration measurements also show low experimental variability. The coefficients of variation remain below 3% for all formulations, for both nitrates and sulfates. This low dispersion confirms the reproducibility of the diffusion experimental setup and indicates that the differences observed between formulations are mainly attributable to variations in concrete composition.

To provide an overall view of result dispersion, the ranges of standard deviations and coefficients of variation observed for each property are summarized in Table 9.

Table 9. Summary of experimental variability of the different measured properties.

Property	Standard Deviation Range	CV Range (%)
Compressive Strength (90 Days)	0.37 - 0.59 MPa	1.43 - 1.83
Water-Accessible Porosity (90 Days)	0.10% - 0.20%	1.11 - 1.85
Water Absorption (90 Days)	0.15% - 0.28%	1.52 - 1.88
Bulk Density (90 Days)	0.010 - 0.020 g/cm^3	0.40 - 0.84
Nitrate Concentrations (Week 12)	0.02 - 0.04 mg/L	1.74 - 2.40
Sulfate Concentrations (Week 12)	0.01 - 11 mg/L	1.95 - 2.78

The statistical analysis shows that the coefficients of variation range from 0.40% to 2.78%, depending on the property considered. These values remain well below the commonly accepted threshold of 5% for cement-based material testing and indicate excellent experimental reproducibility. The low standard deviations observed confirm the stability of the applied protocols. Consequently, the ranking of the formulations established based on physical, mechanical, and ionic transport properties can be considered statistically robust and representative of the actual behavior of the studied materials.

The individual values obtained from the experimental repetitions (n = 3) for compressive strength, water-accessible porosity, water absorption, bulk density, as well as nitrate and sulfate concentrations, are presented in Appendices A1, A2, A3, A4, A5 and A6.. These data allow verification of the calculation of means, standard deviations, and coefficients of variation reported in the summary tables.

4. Discussion

EN 206 provides the reference framework for defining durability requirements for concrete according to environmental exposure classes. In the case of the buried water tanks investigated in this study, the conditions mainly correspond to XC2/XC3 classes, associated with humid environments, as well as XA1 to XA3 classes, which are characteristic of chemically aggressive environments in the presence of nitrates and sulfates. This classification is based on the content of soluble sulfates in soils (XA1: 200 - 600 mg/kg SO_4, XA2: 600 - 3000 mg/kg SO_4, XA3: > 3000 mg/kg SO_4) as well as the concentration of aggressive species in water (pH, aggressive CO_2, magnesium, dissolved sulfates), in accordance with Annex D of the standard [25]. The associated requirements are based on global parameters—water-to-cement ratio (W/C), strength class, and composition—intended to ensure a sufficiently dense microstructure to limit ionic transport.

However, these criteria remain indirect and do not explicitly describe the fundamental mechanisms of transport and reaction within the cementitious matrix [26]-[29]. Numerous studies have shown that durability against chemical attack does not depend solely on initial compactness, but also on the physicochemical evolution of the material under service conditions, particularly due to the interac-

tions between ionic transport and chemical reactions [30]-[32].

The experimental results obtained in this study confirm these limitations. Although the investigated formulations generally comply with EN 206 requirements (W/C between 0.47 and 0.49 and strength classes ≥ C30/37), significant differences in ionic transport behavior were observed. This finding is consistent with the conclusions of [4], which state that the W/C ratio, although correlated with capillary porosity, is not a sufficient indicator of durability. Indeed, concretes that are similar from a normative standpoint may exhibit significantly different diffusivities due to variations in pore network connectivity and tortuosity [33]-[35].

The use of nitrate ions as conservative tracers made it possible to directly characterize the ionic permeability of the materials. The low diffusion coefficients measured for formulations F1 and F3 (Deff ≈ 10^{-11} m^2/s) reflect a dense and poorly connected microstructure, in agreement with studies highlighting the decisive role of connected porosity and tortuosity in controlling diffusive transport processes [27] [33] [36]. These observations confirm that durability results from a strong coupling between transport properties and chemical reactivity, as also demonstrated in [37].

The use of nitrate ions as conservative tracers made it possible to directly characterize the ionic permeability of the materials. The low nitrate concentrations measured for formulations F1 and F3, together with their lowest accessible porosities (8.2% - 8.4% at 90 days), reflect a dense and poorly connected microstructure, consistent with studies highlighting the key role of connected porosity and tortuosity in controlling diffusive transport processes [29] [31] [36]. These results confirm that resistance to nitrate penetration is primarily governed by the transport properties of the material, which are closely linked to its pore microstructure. Thus, the most compact formulations exhibit a better ability to limit nitrate ion migration through the cementitious matrix [33].

The comparative analysis of the formulations reveals strongly contrasting behaviors. Formulations F1 to F4 and F7 - F8, characterized by low porosity, exhibit transport that remains diffusion-controlled but is slowed by the weak connectivity of the pore network. This results in partial retention of nitrate ions within the matrix and lower measured concentrations.

Conversely, formulations F5 and F6 exhibit more pronounced diffusive transport, associated with higher porosity, which limits their performance in terms of durability. These results are consistent with the work of [38] [39], and more recently Winslow *et al.* [40] and Basheer *et al.* [41], who emphasize the importance of transport properties for a realistic assessment of durability, particularly in nitrate-rich environments.

These observations highlight a structural limitation of current prescriptive approaches: EN 206, which is based on global parameters, does not allow discrimination between microstructural states that are nevertheless decisive for actual durability. Thus, concretes that are equivalent according to standards may exhibit significantly different behaviors under service conditions, as also discussed by Al-

exander *et al.* [26] and DuraCrete [42].

In this context, the results obtained in this study align with the transition toward performance-based approaches, such as those proposed by the fib Model Code [43], which rely on physically interpretable indicators. However, the operational consideration of coupled diffusion-reaction phenomena remains limited due to the complexity of interactions between microstructure, transport, and chemistry [44]-[46].

Furthermore, detailed analysis of the results reveals three distinct regimes governing sulfate ion transport in the studied cementitious matrices, reflecting different balances between diffusion, chemical reactions, and internal ion production.

The first regime, illustrated by formulation F6, corresponds to a diffusion-dominated behavior. The agreement between experimental data and the model indicates that transport is primarily governed by concentration gradients, with no significant contribution from chemical reactions. This behavior is characteristic of highly connected porous matrices, in accordance with classical diffusion models in cementitious materials [33] [47].

The second regime, observed for formulation F5, highlights a coupling between diffusion and chemical reactions. The stabilization of concentrations over time reflects partial consumption of sulfate ions through interactions with hydrated phases. The introduction of a kinetic term allows this dynamic to be reproduced, revealing a balance between transport and reactivity, in agreement with the work of Saetta *et al.* [34] and Ulm *et al.* [48].

The third regime, which is predominant (F1 - F4, F7, and F8), is characterized by high concentrations at early ages, indicating the presence of internal sulfate sources. Formulation F8 illustrates a quasi-steady-state leaching regime, corresponding to a balance between internal release and outward flux. This behavior reflects a complex coupling between diffusion, chemical reactions, and leaching of the cementitious matrix. It requires the explicit introduction of a source term for accurate modeling, as shown by Carde *et al.* [49], Atkinson [50], and more recently Steefel *et al.* [51] and Cherif *et al.* [46].

Overall, the diversity of the observed behaviors does not arise from distinct mechanisms, but rather from a redistribution of the relative contributions of diffusion, reaction, and internal production, governed by the intrinsic properties of the microstructure.

In conclusion, these results confirm that durability cannot be reliably assessed within a purely prescriptive framework. A relevant approach requires physically based modeling that explicitly integrates microstructure, ionic transport, and chemical reactivity. Such an approach appears essential for improving long-term predictions of concrete behavior in chemically aggressive environments.

5. Conclusions

This study focuses on the characterization of the physico-mechanical properties

and diffusive behavior of eight (8) concrete mixtures made with local aggregates, in a humid and polluted environment. The results highlight the decisive influence of mix design and microstructure on durability and ionic transport mechanisms. The most efficient concretes are distinguished by low porosity and a more compact microstructure, which improves both mechanical strength and resistance to ion diffusion.

Nitrate transport appears to be primarily governed by diffusion and strongly linked to connected porosity, whereas sulfate transport results from more complex mechanisms combining diffusion, chemical reactions, and leaching. The study thus emphasizes that concrete behavior is closely dependent on mix design parameters, which simultaneously influence pore structure, transport properties, and chemical reactivity.

Finally, these results highlight the need for a multi-criteria and performance-based approach to the design of durable concretes, particularly in chemically aggressive environments, while promoting the use of locally available materials adapted to the studied context.

Conflicts of Interest

The authors declare no conflicts of interest regarding the publication of this paper.

References

[1] Makela, J.B., Ebata-Ndion, B., Malanda, N. and Mbeke, S.K. (2025) Prospective Study and Physico-Mechanical Characterisation of Granular Materials Used in the Manufacture of Ordinary Concrete in Congo. *Geomaterials*, **15**, 1-24. https://doi.org/10.4236/gm.2025.151001

[2] Makela, J.B., Ceti, C.A.M., Sodjinou, R.D., Mfoutou, N.N. and Malanda, N. (2026) Microstructural Study of Common Concrete Manufactured in Congo-Brazzaville. *Open Journal of Civil Engineering*, **16**, 37-59. https://doi.org/10.4236/ojce.2026.161003

[3] Mehta, P.K. and Monteiro, P.J.M. (2014) Concrete: Microstructure, Properties, and Materials. 4th Edition, McGraw-Hill Education.

[4] Neville, A.M. (2011) Properties of Concrete. 5th Edition, Pearson Education.

[5] Malanda, N., Ndion, B.E., Tathy, C., Mongo, T. and Louzolokimbembe, P. (2024) Identification of the Diffusion Coefficients of Pollutants (NO_3^- and Mn^{2+}) through the Walls of Concrete Tank and Vulnerability of the Stored Water Quality. *Engineering*, **16**, 246-274. https://doi.org/10.4236/eng.2024.169019

[6] Taylor, H.F.W. (1997) Cement Chemistry. 2e Edition, Thomas Telford.

[7] Skalny, J., Marchand, J. and Odler, I. (2002) Sulfate Attack on Concrete. Spon Press.

[8] Marchand, J. and Skalny, J. (1999) Materials Science of Concrete: Sulfate Attack Mechanisms. ACS.

[9] Santhanam, M., Cohen, M.D. and Olek, J. (2003) Mechanism of Sulfate Attack: A Fresh Look. *Cement and Concrete Research*, **33**, 341-346. https://doi.org/10.1016/s0008-8846(02)00958-4

[10] Collepardi, M. (2003) A State-of-the-Art Review on Delayed Ettringite Attack on Concrete. *Cement and Concrete Composites*, **25**, 401-407.

https://doi.org/10.1016/s0958-9465(02)00080-x

[11] Neville, A. (2004) The Confused World of Sulfate Attack on Concrete. *Cement and Concrete Research*, **34**, 1275-1296. https://doi.org/10.1016/j.cemconres.2004.04.004

[12] Mehta, P.K. (1993) Concrete in the Marine Environment. E & FN Spon.

[13] Kurdowski, W. (2014) Cement and Concrete Chemistry. Springer.

[14] Malanda, N. (2014) Problème de stockage de l'eau à usage domestique dans les réservoirs en béton armé enterrés sous un sol humide et pollué dans la ville de Brazzaville: Modélisation de la diffusion non linéaire en milieu poreux. Thèse de l'Université Marien N'gouabi.

[15] Tang, L. and Nilsson, L.O. (1992) Chloride Diffusivity in High Strength Concrete at Different Ages. *Nordic Concrete Research*, **11**, 162-171.

[16] Adenot, F. and Buil, M. (1992) Modelling of the Corrosion of the Cement Paste by Deionized Water. *Cement and Concrete Research*, **22**, 489-496. https://doi.org/10.1016/0008-8846(92)90092-a

[17] Scrivener, K.L., Crumbie, A.K. and Laugesen, P. (2004) The Interfacial Transition Zone (ITZ) between Cement Paste and Aggregate in Concrete. *Interface Science*, **12**, 411-421. https://doi.org/10.1023/b:ints.0000042339.92990.4c

[18] Ollivier, J.-P. and Vichot, A. (2014) La durabilité des bétons. Presses de l'ENPC.

[19] Bentz, D.P. and Garboczi, E.J. (1991) Percolation of Phases in a Three-Dimensional Cement Paste Microstructural Model. *Cement and Concrete Research*, **21**, 325-344. https://doi.org/10.1016/0008-8846(91)90014-9

[20] NF EN 12390-2: Essais pour béton durci—Partie 2: Confection et conservation des éprouvettes pour essais de résistance. Saint-Denis La Plaine, France. https://www.boutique.afnor.org/fr-fr/norme/nf-en-123902/essais-pour-beton-durci-partie-2-confection-et-conservation-des-eprouvettes/fa155373/39064=3.977396

[21] NF EN 12390-3: Essais pour béton durci—Partie 3: Résistance à la compression des éprouvettes. Saint-Denis La Plaine, France. https://www.boutique.afnor.org/fr-fr/norme/nf-en-123903/essais-pour-beton-durci-partie-3-resistance-a-la-compression-des-eprouvettes/fa185295/39713

[22] NF P 18-459: Béton—Essais sur béton durci—Mesure de l'absorption d'eau par immersion et détermination de la porosité accessible à l'eau. Saint-Denis La Plaine, France. https://www.boutique.afnor.org/fr-fr/norme/nf-p18-459/beton-essais-sur-beton-durci-mesure-de-labsorption-deau-par-immersion-et-determination-de-la-porosite-accessible-a-leau/fa198662/4282

[23] HACH (2023) NitraVer® 5 Nitrate Reagent Powder Pillows, Method 8039—Cadmium Reduction Method for Nitrate Determination. Hach Company.

[24] ACI Committee 201 (2016) Guide to Durable Concrete (ACI 201.2R-16). American Concrete Institute.

[25] CEN (2013) EN 206:2013+A1:2016—Concrete—Specification, Performance, Production and Conformity. European Committee for Standardization.

[26] Alexander, M., Bertron, A. and De Belie, N. (2012) Performance of Cement-Based Materials in Aggressive Aqueous Environments. Springer.

[27] Baroghel-Bouny, V. (2007) Water Vapour Sorption Experiments on Hardened Cementitious Materials. Part I—Essential Tool for Analysis of Hygral Behaviour and Its Relation to Pore Structure. *Cement and Concrete Research*, **37**, 414-437. https://doi.org/10.1016/j.cemconres.2006.11.019

[28] Jennings, H.M. (2000) A Model for the Microstructure of Calcium Silicate Hydrate in Cement Paste. *Cement and Concrete Research*, **30**, 101-116. https://doi.org/10.1016/s0008-8846(99)00209-4

[29] Thomas, M.D.A. and Bentz, E.C. (2002) Computer Program for Predicting the Service Life and Durability of Reinforced Concrete Exposed to Chlorides. Life-365 Consortium. https://life-365.org/

[30] Samson, E. and Marchand, J. (2007) Modeling the Transport of Ions in Unsaturated Cement-Based Materials. *Computational Materials Science*, **38**, 559-569.

[31] Bary, B. and Sellier, A. (2004) Coupled Moisture—Carbon Dioxide-Calcium Transfer Model for Carbonation of Concrete. *Cement and Concrete Research*, **34**, 1859-1872. https://doi.org/10.1016/j.cemconres.2004.01.025

[32] Lothenbach, B., Le Saout, G., Gallucci, E. and Scrivener, K. (2008) Influence of Limestone on the Hydration of Portland Cements. *Cement and Concrete Research*, **38**, 848-860. https://doi.org/10.1016/j.cemconres.2008.01.002

[33] Garboczi, E.J. (1990) Permeability, Diffusivity, and Microstructural Parameters: A Critical Review. *Cement and Concrete Research*, **20**, 591-601. https://doi.org/10.1016/0008-8846(90)90101-3

[34] Saetta, A., Scotta, R. and Vitaliani, R. (1998) Mechanical Behavior of Concrete under Physical-Chemical Attacks. *Journal of Engineering Mechanics*, **124**, 1100-1109. https://doi.org/10.1061/(asce)0733-9399(1998)124:10(1100)

[35] Mindess, S., Young, J.F. and Darwin, D. (2003) Concrete. 2nd Edition, Prentice Hall.

[36] Promentilla, M.A.B., Sugiyama, T., Hitomi, T. and Takeda, N. (2009) Quantification of Tortuosity in Hardened Cement Pastes Using Synchrotron-Based X-Ray Computed Microtomography. *Cement and Concrete Research*, **39**, 548-557. https://doi.org/10.1016/j.cemconres.2009.03.005

[37] De Weerdt, K., Haha, M.B., Le Saout, G., Kjellsen, K.O., Justnes, H. and Lothenbach, B. (2011) Hydration Mechanisms of Ternary Portland Cements Containing Limestone Powder and Fly Ash. *Cement and Concrete Research*, **41**, 279-291. https://doi.org/10.1016/j.cemconres.2010.11.014

[38] Castellote, M., Andrade, C. and Alonso, C. (2001) Measurement of the Steady and Non-Steady-State Chloride Diffusion Coefficients in a Migration Test by Means of Monitoring the Conductivity in the Anolyte Chamber. Comparison with Natural Diffusion Tests. *Cement and Concrete Research*, **31**, 1411-1420. https://doi.org/10.1016/s0008-8846(01)00562-2

[39] Tang, L. and Nilsson, L.-O. (1993) Rapid Determination of the Chloride Diffusivity in Concrete by Applying an Electric Field. *ACI Materials Journal*, **89**, 49-53. https://doi.org/10.14359/1244

[40] Winslow, D.N., Cohen, M.D., Bentz, D.P., Snyder, K.A. and Garboczi, E.J. (1994) Percolation and Pore Structure in Mortars and Concrete. Cement and Concrete Research, 24, 25-37. https://doi.org/10.1016/0008-8846(94)90079-5

[41] Basheer, L., Kropp, J. and Cleland, D.J. (2001) Assessment of the Durability of Concrete from Its Permeation Properties: A Review. *Construction and Building Materials*, **15**, 93-103. https://doi.org/10.1016/s0950-0618(00)00058-1

[42] DuraCrete (2000) Probabilistic Performance-Based Durability Design of Concrete Structures (Final Report). European Union, Brite EuRam III.

[43] Fib (2013) Fib Model Code for Concrete Structures 2010. Wiley. https://doi.org/10.1002/9783433604090

[44] Samson, E. and Marchand, J. (2007) Modeling the Transport of Ions in Unsaturated

Cement-Based Materials. *Computers & Structures*, **85**, 1740-1756. https://doi.org/10.1016/j.compstruc.2007.04.008

[45] Sharmilan, S., Stang, H. and Michel, A. (2022) A Multi-Species Reactive Transport Model Based on Ion-Solid Phase Interaction for Saturated Cement-Based Materials. *Cement and Concrete Research*, **159**, Article 106861. https://doi.org/10.1016/j.cemconres.2022.106861

[46] Cherif, R., Hamami, A.E.A., Aït-Mokhtar, A. and Bosschaerts, W. (2022) Thermodynamic Equilibria-Based Modelling of Reactive Chloride Transport in Blended Cementitious Materials. *Cement and Concrete Research*, **156**, Article 106770. https://doi.org/10.1016/j.cemconres.2022.106770

[47] Saetta, A.V., Scotta, R.V. and Vitaliani, R.V. (1993) Analysis of Chloride Diffusion into Partially Saturated Concrete. *ACI Materials Journal*, **90**, 441-451.

[48] Ulm, F., Coussy, O., Kefei, L. and Larive, C. (2000) Thermo-Chemo-Mechanics of ASR Expansion in Concrete Structures. *Journal of Engineering Mechanics*, **126**, 233-242. https://doi.org/10.1061/(asce)0733-9399(2000)126:3(233)

[49] Carde, C. and François, R. (1999) Modelling the Loss of Strength and Porosity Increase Due to the Leaching of Cement Pastes. *Cement and Concrete Composites*, **21**, 181-188. https://doi.org/10.1016/s0958-9465(98)00046-8

[50] Alan Atkinson, A. (1985) The Time Dependence of pH within a Repository for Radioactive Waste Disposal. UK Atomic Energy Authority Report.

[51] Steefel, C., Depaolo, D. and Lichtner, P. (2005) Reactive Transport Modeling: An Essential Tool and a New Research Approach for the Earth Sciences. *Earth and Planetary Science Letters*, **240**, 539-558. https://doi.org/10.1016/j.epsl.2005.09.017

Appendix

Table A1. Compressive strength measurement results (n = 3).

Formulation	Specimen 1 (MPa)	Specimen 2 (MPa)	Specimen 3 (MPa)	Mean (MPa)	Standard Deviation (MPa)	CV (%)
F1	36.55	37.18	37.66	37.13	0.56	1.51
F2	28.91	29.26	29.79	29.32	0.44	1.50
F3	39.89	40.34	41.06	40.43	0.59	1.46
F4	29.46	29.93	30.55	29.98	0.55	1.83
F5	24.71	25.01	25.52	25.08	0.41	1.63
F6	22.55	22.82	23.27	22.88	0.37	1.62
F7	31.68	32.09	32.59	32.12	0.46	1.43
F8	32.21	32.58	33.22	32.67	0.51	1.56

Table A2. Water-accessible porosity measurement results at 90 days (n = 3).

Formulation	Specimen 1 (%)	Specimen 2 (%)	Specimen 3 (%)	Mean (%)	Standard Deviation (%)	CV (%)
F1	8.29	8.41	8.50	8.40	0.11	1.31
F2	10.04	10.28	10.29	10.20	0.14	1.37
F3	8.10	8.17	8.33	8.20	0.12	1.46
F4	9.27	9.36	9.57	9.40	0.15	1.60
F5	10.62	10.77	11.01	10.80	0.20	1.85
F6	14.02	14.16	14.42	14.20	0.20	1.41
F7	9.08	9.17	9.35	9.20	0.14	1.52
F8	8.89	9.02	9.09	9.00	0.10	1.11

Table A3. Water absorption measurement results at 90 days (n = 3).

Formulation	Specimen 1 (%)	Specimen 2 (%)	Specimen 3 (%)	Mean (%)	Standard Deviation (%)	CV (%)
F1	8.99	9.08	9.29	9.12	0.15	1.64
F2	11.04	11.18	11.38	11.20	0.17	1.52
F3	8.91	9.01	9.23	9.05	0.17	1.88
F4	10.35	10.48	10.73	10.52	0.19	1.81
F5	12.07	12.20	12.48	12.25	0.21	1.71
F6	15.95	16.15	16.50	16.20	0.28	1.73
F7	10.08	10.21	10.46	10.25	0.19	1.85
F8	9.80	9.92	10.13	9.95	0.17	1.71

Table A4. Bulk density measurement results at 90 days (n = 3).

Formulation	Specimen 1	Specimen 2	Specimen 3	Mean	Standard Deviation	CV (%)
F1	2.42	2.44	2.43	2.43	0.010	0.41
F2	2.35	2.39	2.37	2.37	0.020	0.84
F3	2.40	2.44	2.42	2.42	0.020	0.83
F4	2.38	2.39	2.40	2.39	0.010	0.42
F5	2.34	2.35	2.36	2.35	0.010	0.43
F6	2.27	2.30	2.27	2.28	0.017	0.75
F7	2.40	2.42	2.41	2.41	0.010	0.41
F8	2.39	2.41	2.40	2.40	0.010	0.4

Table A5. Nitrate measurement results at week 12 (n = 3).

Formulation	Specimen 1 (mg/L)	Specimen 2 (mg/L)	Specimen 3 (mg/L)	Mean (mg/L)	Standard Deviation (mg/L)	CV (%)
F1	0.99	1.01	1.03	1.01	0.02	1.98
F2	1.41	1.44	1.47	1.44	0.03	2.08
F3	0.95	0.97	0.99	0.97	0.02	2.06
F4	1.22	1.25	1.28	1.25	0.03	2.40
F5	1.60	1.63	1.66	1.63	0.03	1.84
F6	1.84	1.88	1.92	1.88	0.04	2.13
F7	1.13	1.15	1.17	1.15	0.02	1.74
F8	1.05	1.07	1.09	1.07	0.02	1.87

Table A6. Sulfate measurement results at week 12 (n = 3).

Formulation	Specimen 1	Specimen 2	Specimen 3	Mean	Standard Deviation	CV (%)
F1	151	154	157	154	3.0	1.95
F2	452	460	468	460	8.0	1.74
F3	119	122	125	122	3.0	2.46
F4	423	430	437	430	7.0	1.63
F5	0.35	0.36	0.37	0.36	0.01	2.78
F6	35	36	37	36	1.0	2.78
F7	550	560	570	560	10.0	1.79
F8	177	180	183	180	3.0	1.67